npg

RESEARCH

Implementation of a generalized TACT® algorithm for arbitrary source-object distances

NI Linnenbrügger*[1,2,3], RL Webber[1,2] and TM Lehmann[3]

[1]*Department of Dentistry, Wake Forest University School of Medicine, Winston-Salem, North Carolina, USA;* [2]*Department of Medical Engineering, Wake Forest University School of Medicine, Winston-Salem, North Carolina, USA;* [3]*Institute of Medical Informatics, Aachen University of Technology (RWTH), Aachen, Germany*

Objectives: To implement, refine, and evaluate a generalized TACT reconstruction method that corrects for misregistration caused by uncontrolled variations in projective magnification, alleviates normalization artifacts at borders of backprojections, and exploits all available source information to minimize losses produced from projective truncations in three dimensions.

Methods: A new Java™-based software application was designed and tested *in vitro* using clinically representative data derived from four titanium dental implants in a cadaver jaw segment. These implants were irradiated by an intra-oral X-ray machine from various angles and distances using a solid-state sensor producing 48 radiographs. Six radiopaque markers were attached to the segment facilitating inference of associated projection geometries from analyses of the distributions of their respective shadows as seen by the sensor. Three-dimensional (3D) images were produced using the new algorithm, and the results were compared with those obtained from existing code.

Results: Slices processed using the new program were corrected for magnification errors. The resulting 3D displays showed significantly reduced tomosynthetic blur relative to uncorrected counterparts. The new reconstructions also minimized known border artifacts and made use of all available information. These images demonstrated apparent details otherwise hidden or lost when comparably processed using the control algorithm.

Conclusions: The new software reduces both misregistration and scaling artifacts in tomosynthetically reconstructed slices. Hence, these modifications are expected to increase diagnostic accuracy and facilitate the appropriate application of TACT to an enlarged set of diagnostic tasks as compared with earlier implementations of the method.

Dentomaxillofacial Radiology (2002) **31,** 249–256. doi:10.1038/sj.dmfr.4600703

Keywords: tomography, X-ray computed; image processing, computer-assisted; radiography, dental, digital; artifacts

Introduction

Classical tomosynthetic reconstruction requires all source projections to be constrained to geometries yielding a single fixed magnification.[1] This same basic scaling restriction also applies to the appropriate application of the simplest Tuned-Aperture Computed Tomography® (TACT®) algorithm as implemented by first-generation TACT software.[2,3] Nonetheless, diagnostic quality of TACT imaging has recently been reported for various applications such as the detection of caries, mandibular fractures, and periodontal bone gain as well as cross-sectional presurgical implant planning.[4–7]

Projecting from unconstrained source-object and/or source-detector distances degrades resultant tomosynthetic slices because objects projected with differing magnifications cannot be registered precisely. Two approaches reported previously use information derived from known fiducial relationships to infer projection geometry and consequently determine the appropriate scale-correction factors for each projection.[8,9] However, the first was constrained to a subset of potential applications having limited projection flexibility, and the second was never completely

implemented owing to intrinsic limitations in the first-generation software available at the time. These software limitations were not just limited to problems associated with scaling inaccuracies. Other arbitrary constraints resulted in truncation of projection data in most slice reconstructions and the introduction of artifacts attributable to inappropriate normalization of contrast.

This article documents our efforts to eliminate these acknowledged shortcomings through the creation of a second-generation software package. The new 32-bit program called TactJ is written in JAVA allowing it to run on virtually any computer platform without the assignable memory constraints present in the original (16-bit) TACT Workbench. Our intent was to seamlessly incorporate both the flexibility and scaling accuracy as described by Robinson *et al*.[9] into a usable package that can accommodate virtually any desired projection geometry. More specifically, the aim of this study is to test this new software package through controlled representative comparisons designed to demonstrate the extent of circumvented constraints and enhancements relative to the prior (first-generation) TACT algorithms.

Theory

TACT is a method that generates three-dimensional (3D) images from a series of arbitrarily oriented, two-dimensional (2D) projections by synthesizing underlying projection geometries retrospectively using information inferred from projections of recognizable fiducial patterns. A common variant of the method makes use of extrinsically applied radiopaque spheres that are rigidly attached to the irradiated object near the region of interest. When properly distributed, the centers of projected shadows produced from these spheres serve as easily recognized fiducial points. If their patterns fulfill appropriate mathematical criteria, this method can determine both angle and magnification of any arbitrary radiographic projection from analysis of the associated 2D projection patterns.[10,11]

A rigorous mathematical foundation for TACT proved that six distinct reference points fixed to the object under examination are sufficient to uniquely reconstruct projection geometry in the perfectly general case, wherein the object can arbitrarily move relative to the detector and no restrictions apply to the source–object relationship.[9] Qualitatively, one reference point is required for the application of the original TACT algorithm,[2] another one is needed if the source–object distance is variable, and another four enable the object and radiation sensor to be decoupled. A convenient embodiment allows four of the points to be coplanar and the other two points determining a line parallel to (but not contained in) the plane defined by the four points[9] (Figure 1). Practically, this perfectly general case is solved by first solving for projective transformations that map the shadows of the four coplanar points in
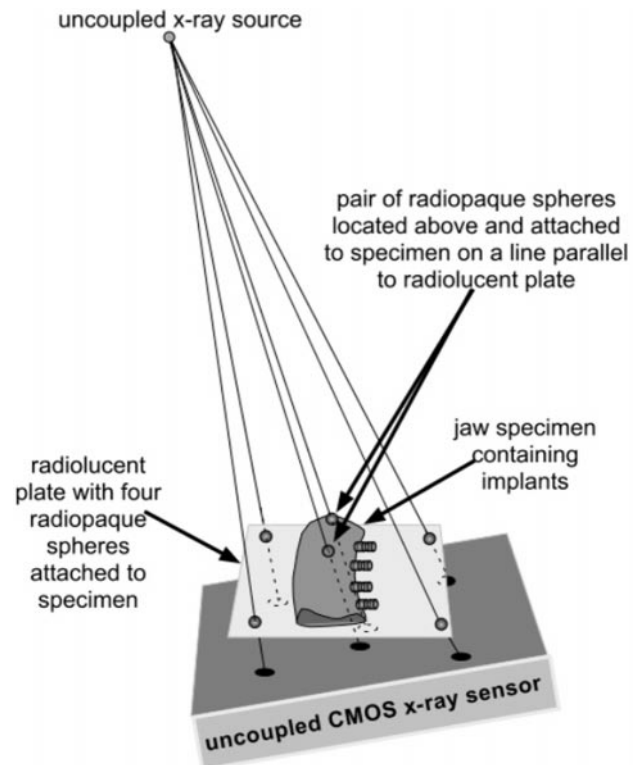

Figure 1 Schematic diagram of the geometry used to create arbitrary projections for generalized tomosynthetic reconstruction

each projection to a common set of four reference points. The application of these transformations is conceptually equal to moving the object in such a way that for each projection the plane defined by the four points is on the plane of the detector. Similarly, the orientation of the detector under these conditions is coincident with the plane determined by the four coplanar reference points. Thus, after these projective transformations, the object may be now considered fixed to the detector. All that remains to be completed at this point is the process of scale-corrected tomosynthetic backprojection. This step requires knowledge of the source–detector projection geometry relative to the irradiated object. The generalized TACT algorithm as described by Robinson *et al*.[9] infers this geometry from projections of the remaining two reference points.

Under these conditions, projected images of the spheres on top of the object shift laterally with changes in the angle of the source relative to the now-fixed sensor plane, and the distance between them changes with variations in the proximity of the X-ray source (Figure 2). In the following, shadows of the two spheres fixed to the object will be referred to as 'fiducial references' or simply 'fiducials' because the centers of these shadows can be accurately deduced owing to their relative radiopacity. Knowing the actual distance between the two spheres that are fixed to the object and the spacing of the fiducials enables reliable estimation of the magnification of objects lying in the
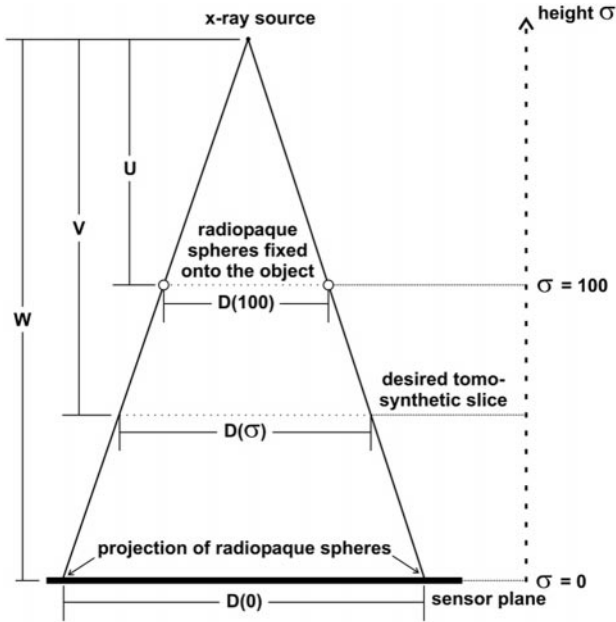
Figure 2 Spatial relations of X-ray source, radiopaque spheres, sensor plane and the desired tomosynthetic slice (auxiliary distances $U - W$ are used in the Appendix only)

plane of the two spheres. Similarly, objects located at a different plane are magnified according to their orthogonal distance to the sensor.

As it can be seen from similar triangles, the magnification of an object is directly proportional to its distance above a projection plane (Figure 2). Thus, using the known magnification at one plane allows one to infer its value for any other plane. To ensure that objects situated at a certain distance above the sensor are correctly scaled, it is necessary to resize each projection prior to reconstruction. Resizing is determined by the position σ of the desired tomosynthetic slice and the magnifications established by the distance between fiducial references on the projection plane in respective projections. By definition, the sensor surface and the reference plane containing the two radiopaque spheres are at height $\sigma = 0$ and $\sigma = 100$, respectively. The magnification correction $C(\sigma)$ for objects that are situated at height σ is given by

$$C(\sigma) := \frac{D(\sigma)}{D(0)} \qquad (1)$$

where $D(\sigma)$ denotes the actual size of an object located at height σ and $D(0)$ is the size of the corresponding shadow of this object on the projection plane. Analogous to (1), the correction-factor $C(100)$ for projective magnification of objects that are located at height $\sigma = 100$ is defined by

$$C(100) := \frac{D(100)}{D(0)} \qquad (2)$$

where $D(100)$ and $D(0)$ denote the distances between the two radiopaque spheres in the reference plane and

the corresponding fiducial references on the sensor surface, respectively. Knowing $C(100)$, the magnification correction for objects situated at height σ can be obtained by

$$C(\sigma) = 1 - \frac{\sigma}{100} + \frac{\sigma}{100} \cdot C(100) \qquad (3)$$

The derivation of (3) is given in the Appendix.

Scaling of projections according to $C(\sigma)$ compensates for projective magnifications so that objects located at a certain tomosynthetic slice position appear properly scaled relative to the actual distance between the two reference spheres. The result is a system that allows the observer to make accurate measurements from the 3D images appropriately scaled in real-world units.

Implementation

Figure 3 summarizes the resulting algorithm. After initialization (lines 01–05), the magnification of objects located at height $\sigma = 100$ is determined by measuring the proximity of the two spheres with a caliper and calculating the corresponding distance $D(100)$ in pixels by means of the known sensor pitch (lines 03–04). Next, all source images, which are acquired without any geometric constraints (line 05), are transformed in such a way that for each projection the plane defined by the four points is on the plane of the detector (lines 06–12). Thereafter, the dimensions of the TACT volume to be reconstructed are determined (line 13).

In line 16, Equation 3 is used to calculate magnification correction-factors $C(\sigma)$ at any tomosynthetic slice position σ based on the correction-factor $C(100)$ applicable to objects in the reference plane ($\sigma = 100$). As one can deduce from Equation 2, the magnification correction-factor $C(100)$ only depends on the observed distance $D(0)$ between fiducials and the

```
01    attach four co-planar fiducial references to the object
02    attach two parallel fiducial references
03    measure the distance between the two fiducials by a caliper
04    calibrate the system
05    acquire arbitrary source projections
06    for all source projections do
07        determine co-planar fiducials' coordinates
08        determine parallel fiducials' coordinates
09        calculate parameters of projective transform
10        transform the image using interpolation
11        remove co-planar fiducials from images
12    od
13    specify range and number of slices
14    for each desired slice position do
15        for all transformed projections do
16            calculate magnification correction
17            re-scale projection
18            shift projection toward the common midpoint
19            if projection does not fit the frame then
20                increase frame size
21        od
22        for each pixel within the final frame do
23            sum up all overlapping projections
24            divide by the number of overlapping projections
25        od
26        store slice
27    od
```

Figure 3 Pseudocode of the generalized TACT algorithm. The major parts, i.e., initialization, projective reconstruction, tomosynthetic backprojection, scale correction, frame adjustment, and normalization, are represented in lines 01–05, 06–12, 13–27, 16–17, 18–20, and 22–25, respectively

actual spacing $D(100)$ between the two radiopaque spheres. Thus, $C(100)$ needs to be computed only once for each projection, whereas $C(\sigma)$ must be calculated individually for each projection and each slice position σ. Note that $C(100)$ and $C(\sigma)$ are relative values wherein a quantity of 0.9 means that a projection has to be scaled down by 10%.

After each projection has been appropriately scaled (line 17), the algorithm shifts the projections toward the common midpoint of the reference points from all projections according to the desired slice position (line 18), as described by Webber *et al*.[2] Notice that this process requires image registration about a single reference point. Existing implementations of TACT calculate and provide only slice information available at the original position of the unprocessed projections and discard information available outside these borders. The method introduced here avoids the loss of this information by dynamically increasing the size of the limiting borders to always encompass the complete ensemble of all the projections after the tomosynthetic shifting has been accomplished (lines 19–20).

All previous TACT algorithms divide every position in a slice by the same denominator, leading to decreasing contrast where fewer projections overlap and sharp edges between areas with different contrasts. We alleviated these problems by keeping track of the number of overlapping projections at each location and normalizing by the correct denominator (lines 22–25). This produces more evenly distributed contrast and smoother transitions between regions where an under-represented number of projections contribute to the superposition.

Materials and methods of evaluation

A segment of an embalmed cadaver mandible with soft tissues intact and containing four titanium intra-osseous implants was radiographed from 48 different positions. The X-ray source was a Siemens Heliodent (Siemens Medical Systems, Iselin, NJ, USA) operating at 60 kVp with 1.5 mm total aluminum equivalent filtration. Images were recorded using empirically selected exposures that lay within the range recommended by the manufacturer of the solid-state digital sensor (Schick Technologies, Long Island City, NY, USA). The latter was a #2-sized CMOS device with a total size of 640×900 pixels in *x*- and *y*-directions, respectively.

The exposures were grouped into four homologous series each corresponding to a different focal-object distance. The distances were evenly distributed across a range varying from 140 mm to 307 mm to assure that a significant range of projective magnifications would be distributed among the resultant radiographic projections. Within each distance, source-object relationships were arbitrarily chosen. The exposure differences that otherwise would be caused by these variations in projection distance were eliminated through compensatory adjustment of exposure time.

Although not required by the method, the jaw segment with its system of fiducial markers was taped to the sensor to assure some measure of control over the range of projections explored in this investigation. The distance between the spheres above the specimen was 7.48 mm, as determined by a vernier caliper. Multiplying this distance by the known pitch of the sensor (25 pixels/mm) yields an absolute value of 187 pixels (corresponds to distance $D(100)$ in Figure 2).

The resultant images were then used to calculate a total of four series (each processed differently) of tomosynthetic slices, where each series consisted of 51 equidistantly spaced slices extending over the whole region between the sensor and the reference spheres on top of the sample. This corresponded to an inter-slice distance of approximately 0.5 mm, as the position of the reference spheres was about 25 mm above the detection plane. These four series are defined below.

(1) *Unoptimized control*: The first series was comprised of slice reconstructions derived from the original TACT reconstruction method.
(2) *Control with expanded format*: The second series is identical to the first except that the reconstruction algorithm did not truncate the window size so that complete 3D information was retained in the display.
(3) *Optimized control*: The third series was characterized by slices that were optimized in that they were produced with appropriate normalization and without truncation losses.
(4) *Optimized & scale-corrected*: The fourth series was similar to *optimized control* except that slices were also compensated for differences in magnification resulting from different focal-object distances.

Corresponding slices through the implant at the far left of the specimen from the first three series (*unoptimized control, control with expanded format*, and *optimized control*) were compared in order to visualize consequences of enhancements that divide by the correct denominator at each location and exploit all available information from projections when reconstructing tomosynthetic slices. To determine the degree to which correction of magnification reduces projective misregistration, corresponding slices at the level of the plane containing the reference spheres in the third and fourth series (*optimized control* and *optimized & scale-corrected*, respectively) were evaluated. Other slices through one of the implants were used to reveal clinical effects of these reconstruction methods on representative images of dental interest. The accuracy of measurements in corrected and uncorrected slice stacks was assessed by comparing the distances between the fiducials in respective tomosynthetic slices with the actual distance deter-
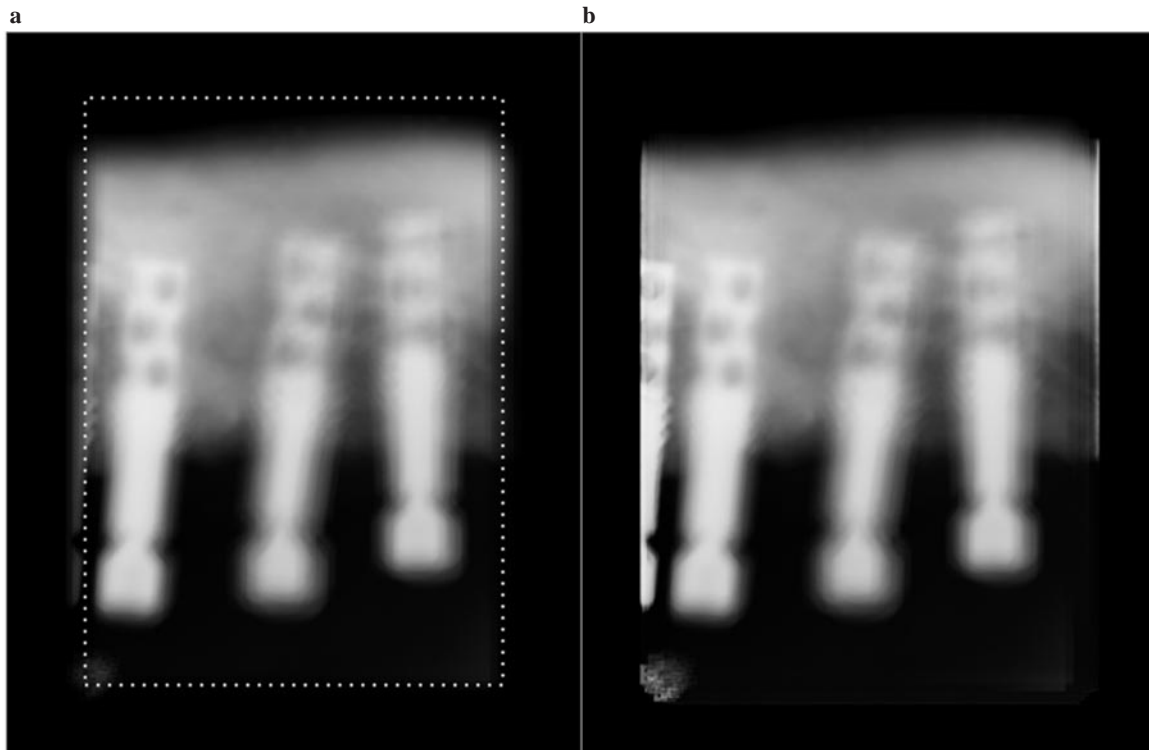
Figure 4 Reconstructed slice through the head of the implant at the far left of the specimen: (a) *control with expanded format* with a dotted frame indicating position and extent of the *unoptimized control* and (b) *optimized control*
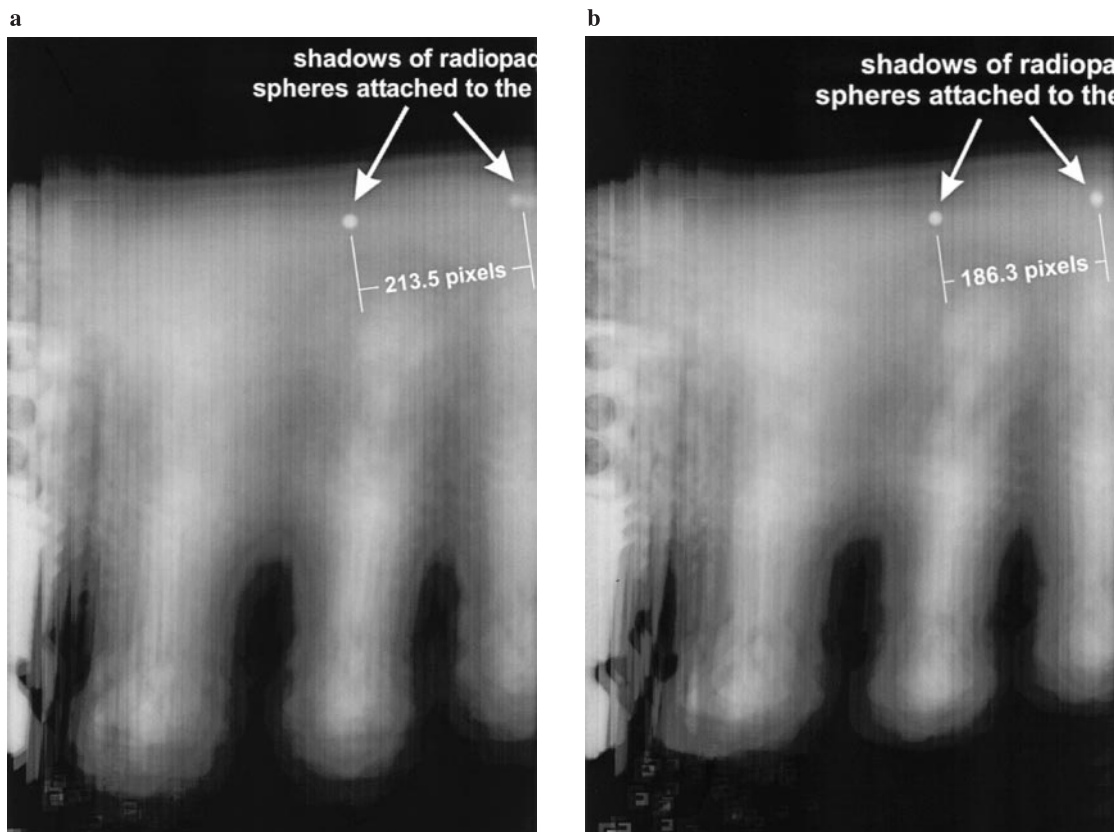

Figure 5 Reconstructed slice through plane containing the reference objects: (a) *optimized control* and (b) *optimized & scale-corrected*

mined by multiplying their spacing in real-world coordinates with the sensor's pitch.

Results

Figure 4 displays slices through the head of the implant at the far left of the specimen when viewed from above. The slice obtained from the *unoptimized control* is restricted in size, blurred, and shows only three of the implants (indicated by a dotted frame in Figure 4a). The slice of *control with expanded format* (Figure 4a) also covers information available at the borders of the underlying projections. Here, also the fourth implant on the left hand side is visible, although under-represented in brightness. The slice corresponding to the *optimized control* (Figure 4b) evidently shows the effect of normalizing pixel brightnesses by dividing by the actual number of overlapping projections. The fourth implant can be clearly seen. The dimensions of the frame are increased to compensate for different slice sizes within a slice stack, which results in a black border region in some reconstructions, as illustrated in Figure 4b.

Figure 5a shows a reconstructed slice through the plane containing the two reference spheres on top of the object under investigation ($\sigma = 100$) produced without correction for variations in projective magni-

fication (*optimized control*). Notice that only the fiducial used as the reference point for backprojection is in perfect registration, and the other one is blurred due to differential magnification of projections that were shifted and added to create this slice. The slice in Figure 5b is at the same position as the slice shown in Figure 5a but has been formed by means of adjusting for different projective magnifications (*optimized & scale-corrected*). Here, the second fiducial is almost perfectly registered as well. The distance between fiducial references in the uncorrected slice shown in Figure 5a has been estimated to be 213.5 pixels, although the position of the second fiducial can only be approximated due to its being blurred. In the scale-corrected slice (Figure 5b), the fiducials have a spacing of 186.3 pixels, which is an almost perfect measure compared to the actual separation of 187 pixels inferred from a real-world measurement and the sensor pitch, as described above.

Figure 6 shows slices through the head of the third implant from the left, when viewed from above, that have been calculated without and with scale-correction demonstrating clinical effects of *optimized control* and *optimized & scale-corrected* reconstruction methods, respectively. Notice the improved details in the bone structure and the increased sharpness of the head of the implant resulting from scale-correction (Figure 6b) compared to its uncorrected counterpart (Figure 6a).
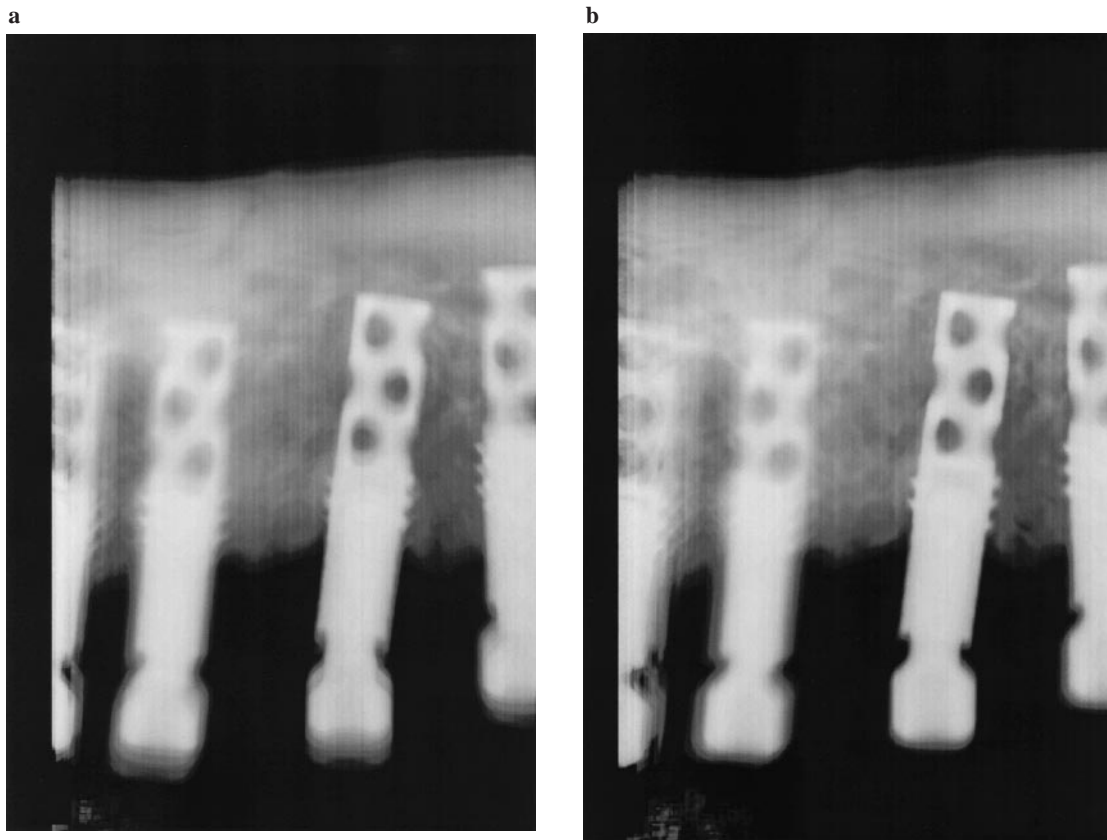

Figure 6 Reconstructed slice through head of third implant from the left: (a) *optimized control* and (b) *optimized & scale-corrected*

Discussion

The progressive algorithmic improvements retain structural information that is completely lost by use of previous TACT algorithms. Notice that the implant at the far left in Figure 4b does not become apparent in any other slice of the control series. It follows that these enhancements promise to provide the practitioner with a superior diagnostic tool when information near the borders of component projections is important. Moreover, these data demonstrate how using a reconstruction scheme that adapts slice sizes according to underlying projection data and properly normalizes contrast over the entire region can reveal potentially significant information that might otherwise be lost.

It is obvious from Figures 5a,b and 6a,b that reconstructed slices not corrected for variations in magnification cannot be registered precisely. This inadequacy is manifest by their significantly increased blur relative to comparable display after scale correction.

The slight blurring of the right fiducial marker relative to the left in Figure 5b, which is manifest predominantly in the vertical direction, is probably caused by the fact that the plane containing the two reference objects was observed not to be perfectly parallel to the detection plane. Although the geometric effect of this slight deviation from the ideal is minimal, insofar as its effect on scale correction is concerned, it would influence the tomographic appearance of these objects when they are not constrained to lie in the same reconstruction plane.

Reconstructed control slices without scale-correction were derived from projections produced at finite focal-object distances, which necessarily yields projective magnifications greater than unity. Consequently, distances determined within such TACT slices are always exaggerated. It has been shown that these errors in distance measures can be eliminated (to an accuracy less than one pixel in the reference plane) by correcting for projective magnifications preceding tomosynthetic slice creation. Hence, with appropriate calibration in the direction orthogonal to the detection plane, one can accurately measure distances between, as well as across, arbitrarily selected slices, so that any desired distance can be determined accurately within the complete 3D volume encompassed by the TACT reconstruction process. Nevertheless, it has to be emphasized that the plane containing the reference objects, i.e., the two radiopaque spheres must be parallel to the projection plane. It has been mentioned that this rather restrictive assumption can be alleviated by fixing the object to a radiolucent plate with four fiducial spheres attached (Figure 1) and placing the two radiopaque spheres on a line parallel to (but not contained in) the plane defined by the four fiducial spheres.[9] Furthermore, the reference distance that expresses the actual spacing of the two spheres in pixels must be accurately determined to ensure precise registration and dimensional accuracy of corrected slice series, irrespective of the actual X-ray source and/or detector positions.

The results demonstrated in Figures 4–6 were obtained without applying any further improvements or optimization techniques. In our current implementation, the tomosynthetic alignment of projections is done for each slice by nearest neighbor interpolation while the correction of magnification is based on linear interpolation. For each TACT slice, the total error induced by interpolation may enlarge with the total number of projections used for TACT reconstruction. In particular, this process blurs local volumes of high contrast, e.g. in peri-implant regions. Hence, we anticipate that the use of B-spline interpolation of high order would essentially improve the quality of TACT reconstructions.[12,13] Furthermore, the impact of other optimization techniques, such as the deconvolution of slices,[14] has already been proven. Note that these optimizations are applicable in addition to and not in place of our techniques.

In conclusion, we have experimentally verified that the new software improves the relative quality of TACT reconstructions by

(1) correcting for variations in magnification attributable to unconstrained projection geometries;
(2) applying region-specific gray-level normalization to eliminate intrinsic contrast errors; and
(3) sample-specific adaptation of reconstruction window size to eliminate all truncation artifacts that would result otherwise.

References

1. Grant DG. Tomosynthesis: a three-dimensional radiographic imaging technique. *IEEE Trans Biomed Eng* 1972; **19:** 20–28.
2. Webber RL, Horton RA, Tyndall DA, Ludlow JB. Tuned-aperture computed tomography (TACT^TM). Theory and application for three-dimensional dento-alveolar imaging. *Dentomaxillofac Radiol* 1997; **26:** 53–62.
3. Horton RA. TACT Workbench: image processing application for tuned-aperture computed tomography, Copyright 1993–2001. Verity Software Systems, Winston-Salem, NC.
4. Shi XQ, Han P, Welander U, Angmar-Månsson B. Tuned-aperture computed tomography for detection of occlusal caries. *Dentomaxillofac Radiol* 2001; **30:** 45–49.
5. Nair MK, Webber RL, Johnson MP. Comparative evaluation of Tuned Aperture Computed Tomography^® for the detection of mandibular fractures. *Dentomaxillofac Radiol* 2000; **29:** 297–301.
6. Chai-U-Dom O, Ludlow JB, Tyndall DA, Webber RL. Detection of simulated periodontal bone gain by digital subtraction radiography with tuned-aperture computed tomography. The effect of angular disparity. *Dentomaxillofac Radiol* 2001; **30:** 92–97.

7. Liang H, Tyndall DA, Ludlow JB, Lang LA. Cross-sectional presurgical implant imaging using tuned aperture computed tomography (TACT^{TM}). *Dentomaxillofac Radiol* 1999; **28:** 232 – 237.

8. Webber RL, Bettermann W. A method for correcting for errors produced by variable magnification in three-dimensional tuned-aperture computed tomography. *Dentomaxillofac Radiol* 1999; **28:** 305 – 310.

9. Robinson SB, Hemler PF, Webber RL. A geometric problem in medical imaging. *Proceedings of SPIE* 2000; **4121:** 208 – 217.

10. Webber RL (inventor; Wake Forest University, assignee). Self-calibrated tomosynthetic radiographic-imaging system, method, and device. US patent 5,359,637. 1994, Oct 25.

11. Webber RL (inventor; Wake Forest University, assignee). Self-calibrated tomosynthetic radiographic-imaging system, method, and device. US patent 5,668,844. 1997, Sept 16.

12. Lehmann TM, Gönner C, Spitzer K. Survey: Interpolation methods in medical image processing. *IEEE Trans Med Imag* 1999; **18:** 1049 – 1075.

13. Lehmann TM, Gönner C, Spitzer K. Addendum: B-spline interpolation in medical image processing. *IEEE Trans Med Imag* 2001; **20:** 660 – 665.

14. Persons TM. *Three dimensional tomosynthetic image restoration for brachytherapy source localization.* PhD Thesis, Wake Forest University. May, 2001.

Appendix

In the following, a derivation of Equation 3, which calculates a correction-factor for projective magnification as a function of the slice position σ, is provided. By definition and observed from similar triangles in Figure 2, we obtain

$$\frac{U}{W} = \frac{D(100)}{D(0)} = C(100) \tag{4}$$

$$\frac{U}{V} = \frac{D(100)}{D(\sigma)} \tag{5}$$

$$V = W - \frac{\sigma}{100} \cdot (W - U) \tag{6}$$

Solving (4) and (5) for $D(100)$, using equalities, substituting (6) into the result, and simplifying yields

$$\frac{D(\sigma)}{D(0)} = 1 - \frac{\sigma}{100} + \frac{\sigma}{100} \cdot \frac{U}{W} \tag{7}$$

Finally, substituting (4) into (7) results in

$$\frac{D(\sigma)}{D(0)} = 1 - \frac{\sigma}{100} + \frac{\sigma}{100} \cdot C(100) \tag{8}$$